Journal of Applied Physics

Effects of the introduction of a chromium oxide monolayer at the C_{60}/Fe(001) interface

Cite as: J. Appl. Phys. **125**, 142907 (2019); https://doi.org/10.1063/1.5075531
Submitted: 23 October 2018 . Accepted: 13 December 2018 . Published Online: 01 April 2019

Alberto Brambilla, Andrea Picone, Simona Achilli, Guido Fratesi, Alessandro Lodesani, Alberto Calloni, Gianlorenzo Bussetti, Maurizio Zani, Marco Finazzi, Lamberto Duò, and Franco Ciccacci

Journal of Applied Physics ARTICLE scitation.org/journal/jap

Effects of the introduction of a chromium oxide monolayer at the C_{60}/Fe(001) interface

Cite as: J. Appl. Phys. **125**, 142907 (2019); doi: 10.1063/1.5075531
Submitted: 23 October 2018 · Accepted: 13 December 2018 ·
Published Online: 1 April 2019

Alberto Brambilla,[1,a)] Andrea Picone,[1] Simona Achilli,[2] Guido Fratesi,[2] Alessandro Lodesani,[1] Alberto Calloni,[1] Gianlorenzo Bussetti,[1] Maurizio Zani,[1] Marco Finazzi,[1] Lamberto Duò,[1] and Franco Ciccacci[1]

AFFILIATIONS

[1]Dipartimento di Fisica, Politecnico di Milano, piazza Leonardo da Vinci, 32-20133 Milano, Italy
[2]ETSF and Dipartimento di Fisica, Università degli Studi di Milano, Via Celoria, 16, 20133 Milano, Italy

[a)]**Electronic mail:** alberto.brambilla@polimi.it

ABSTRACT

The introduction of a two-dimensional oxide layer at the interface between an organic semiconductor and a ferromagnetic metal (spinterface) can help in tailoring the formation of spin-polarized hybridized interface states. Here, we consider the case of a Cr_4O_5 monolayer at the C_{60}/Fe(001) interface, which is already known to feature the occurrence of spin-polarized states in the fullerene molecules. In this work, we employ scanning tunneling microscopy/spectroscopy and photoemission spectroscopy to show that the C_{60}/Cr_4O_5/Fe(001) spinterface is characterized by the formation of a well-ordered fullerene monolayer and of strongly hybridized interface states. These experimental results are discussed in terms of state-of-the-art *ab initio* calculations of the structural, electronic, and magnetic properties at the interface.

I. INTRODUCTION

In the last few years, several experimental and theoretical investigations have suggested that organic materials can achieve comparable, or even enhanced, performances in spin-based devices with respect to inorganic materials, and that they can also provide new concepts, leading to the new field of Organic (or Molecular) Spintronics.[1] The key role in such systems is played by the so-called spinterfaces,[2–4] i.e., interfaces between ferromagnetic (FM) materials, which provide spin-polarized electrons, and organic semiconductors (OS), which are characterized, in particular, by long lifetimes for spin-polarized electrons. It is now commonly understood that the fundamental processes related to spinterfaces, such as the modifications of the magnetic properties of either the OS or the FM layers and the possibility of injecting spins in the organic layer, are governed also by the chemical interactions occurring at the OS/FM interface.[5] For this reason, a detailed control over the interface characteristics is of paramount importance to define and, eventually, tailor physical systems with capabilities of interest for potential applications.

In inorganic spintronic systems, it is well known that the intercalation of thin and ultra-thin oxides in proximity to FM metals (for instance, as tunneling barriers in multilayer junctions) directly influences the magnetic properties of the system, very often with favorable effects.[6] This aspect has not been, so far, thoroughly investigated in Organic Spintronics, even if thin oxide films were already exploited in organic spin valves based on standard spintronic concepts.[7] Recently, we started evaluating the influence of introducing an oxidized layer in a spinterface by comparing the early stages of growth of C_{60} fullerene films onto either the Fe(001) surface or the oxygen-passivated Fe(001)-$p(1 \times 1)$O surface.[8] We were able to show that the oxygen passivation of the Fe(001) surface, which results in the formation of an FeO-like monolayer with enhanced spin-dependent properties,[9–11] substantially affects the interface in terms of the growth morphology by changing the molecular surface diffusivity, and of the electronic properties, with a substantial electronic decoupling in the presence of the oxidized layer. We have furthermore studied the magnetic hybridization at such interfaces and at the interface between a C_{60} and a Cr_4O_5 monolayer stabilized onto the Fe(001) surface.[12] Those investigations lead to the observation of spin-polarized fullerene states in all cases.

In this work, we analyze in more detail the C_{60}/Cr_4O_5 spinterface by exploiting combined experimental and theoretical approaches. The interaction of C_{60} molecules with the Cr_4O_5/Fe surface is experimentally characterized by a relatively strong

electronic coupling and by a low diffusion barrier, resulting in a well-ordered fullerene monolayer with strongly hybridized interface states. The experimental observations, based on scanning tunneling microscopy and spectroscopy and on photoemission spectroscopy, are supported by state-of-the-art *ab initio* calculations, used to discuss how the local interaction between the C_{60} molecule and the substrate affects the electronic and magnetic properties of the interface.

II. METHODS

A. Experimental methods

Samples were prepared in ultrahigh vacuum (UHV) (low 10^{-10} mbar range) by growing 400 nm-thick Fe(001) films on MgO (001) single crystal substrates by molecular beam epitaxy (MBE). The Fe surface was first passivated by oxygen to obtain the oxygen-saturated Fe(001)-$p(1 \times 1)$O surface, as described in previous works.[10,13] A Cr_4O_5 monolayer oxide was then prepared by depositing 0.8 equivalent monolayers (MLs) of Cr on top of the Fe(001)-$p(1 \times 1)$O surface, with the sample held at about 400 °C, as measured by a thermocouple mounted in close proximity to the sample position. Such a two-dimensional Cr oxide has been demonstrated to form a stable wetting layer on Fe(001), characterized by a regular array of Cr vacancies that results in a $(\sqrt{5} \times \sqrt{5})-R26.6^\circ$ surface lattice.[14] This system is characterized by a long-range FM order with in-plane magnetization, oriented anti-parallel with respect to that of the Fe substrate.[15,16] Fullerene films were grown onto the Cr_4O_5/Fe substrates by MBE under UHV conditions, with the substrates held at room temperature.

Scanning tunneling microscopy (STM) was performed *in situ* (Omicron VT-STM) in the constant-current mode with homemade electrochemically etched W tips. Scanning tunneling spectroscopy (STS) was performed at liquid nitrogen temperature (sample temperature, about 100 K). Tunneling spectra were obtained by superimposing a modulation voltage (rms amplitude of 20 mV) to the applied sample bias V and detecting the dI/dV signal by a lock-in amplifier.

Photoemission spectroscopy (PES) in the UV range was performed with He I radiation ($h\nu = 21.2$ eV) from a He discharge lamp. Photoelectrons were collected by a 150 mm hemispherical electron analyzer (SPECS GmbH) operated at a pass energy of 0.5 eV (the estimated instrumental resolution is about 0.05 eV full width at half-maximum).[17]

B. Computational methods

The *ab initio* theoretical calculations were performed in the density functional theory (DFT) formalism. We treated the exchange-correlation, accounting for the spin polarization of the system, by exploiting the vdW-DF-c09 functional. This combines the vdW-DF functional[18] with the Cooper gradient correction to the exchange[19] and includes the van der Waals interaction between the C_{60} molecules and the substrate. We adopted the plane-wave ultrasoft pseudopotential method[20] implemented in the PWSCF code of the Quantum-ESPRESSO distribution.[21] Pseudopotentials were generated starting from scalar-relativistic all-electron calculations and using non-linear core corrections. The 3*s*3*p* semi-core states of Cr were included.

The substrate surface geometry is assumed to correspond to the $(\sqrt{5} \times \sqrt{5})-R26.6^\circ$ reconstruction, as experimentally observed for a single Cr_4O_5 layer on Fe(001).[14] The C_{60} molecules were placed in a squared arrangement with a $(\sqrt{10} \times \sqrt{10})-R(-18.4^\circ)$ periodicity, with a surface supercell having a double area with respect to the primitive Cr_4O_5 one. This choice, although not strictly corresponding to the experimentally observed periodicity (see below), allowed us to catch the fundamental aspects of the local molecule-substrate interaction, avoiding an excessive increase of the computational cost. A slab with four Fe layers was used to model the Fe(001) substrate, with the Cr_4O_5 layer and the molecules placed on one side. The periodic replica of the slabs were separated by 25 Å of vacuum along the orthogonal direction z.

We considered different orientations of C_{60}, namely, the ones corresponding to a molecule facing the surface by a hexagonal face, by a C–C bond, and by a pentagonal face, and placing the molecule on top of Cr atoms, Cr vacancies, and O atoms farthest from the vacancies. Once the system was prepared in these local configurations, the z coordinate of the carbon atoms was left free to relax until the forces reached the limiting value of 0.001 Ry/bohr.

The surface Brillouin zone was sampled by a Monkhorst-Pack grid[22] equivalent to a 14×14 mesh in the surface unit cell of Fe (001). The kinetic energy cutoffs are 55 Ry for the wave function and 280 Ry for the effective potential and the charge density.

III. RESULTS AND DISCUSSION

Figure 1(a) displays a large scale STM image acquired after the deposition of about 1 ML C_{60} on the Cr_4O_5 surface. The molecules form a compact and homogeneous monolayer, wetting the substrate, with only a small portion of second layer forming upon completion of the first one (brighter areas in the STM image). Panel (b) displays the Fast Fourier Transform of the STM image, in which two hexagonal lattices mutually rotated by 90° are detected. The presence of two rotational domains stems from the fourfold symmetry of the substrate and indicates that there is a well-defined epitaxial relation between the latter and the molecular overlayer. In particular, in each domain, one unit vector of the C_{60} lattice is aligned with either the [100] or the [010] crystallographic direction of the Fe(001) surface. A quantitative evaluation of the peak-peak separation in the reciprocal space, reported in the profile corresponding to the red dashed line drawn in the inset of panel (b), yields a real space lattice parameter of 1.03 nm, a value in good agreement with that characterizing the (111) surface of bulk face-centered-cubic C_{60}.[23] Panel (c) shows an enlarged view of the C_{60} overlayer, in which a boundary region between two domains is visible. Two white parallelograms are drawn to highlight the unit cells in the adjacent domains.

The curve in panel (d) has been obtained by averaging several STS spectra acquired on the C_{60} wetting layer. In the occupied states side of the spectrum (negative bias), a broad feature at about 2 eV below the Fermi level E_F is detected, which can be assigned to HOMO states. On the unoccupied states side (positive bias), a peak corresponding to the LUMO level can be observed at about 1 eV above E_F.

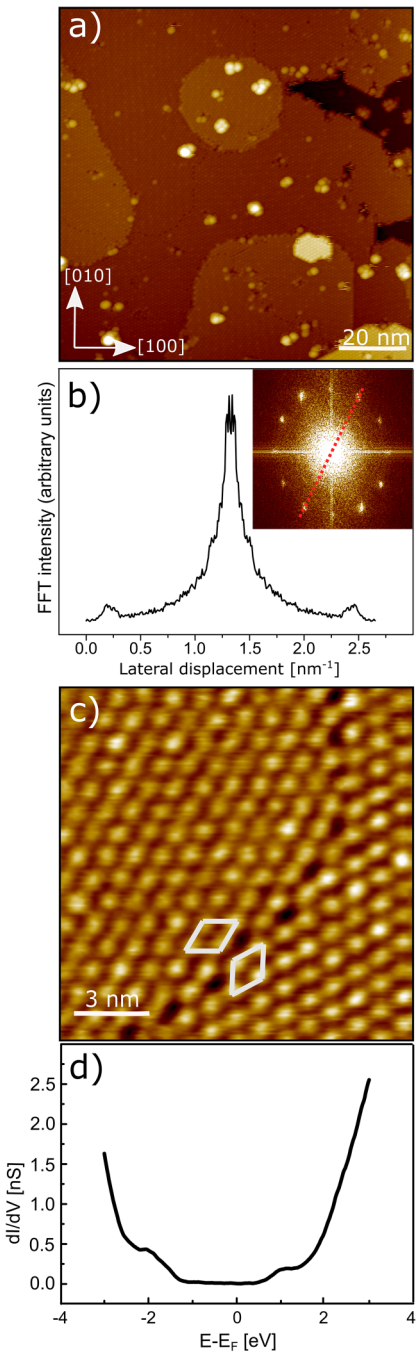

FIG. 1. (a) STM image of 1 ML C_{60} on Cr_4O_5/Fe. Image size is $105 \times 105\,nm^2$. Tunneling parameters $\Delta V = 1.7\,V$, $I = 400\,pA$. (b) Fast Fourier Transform of panel (a), in which two orthogonal hexagonal domains are observed. The side of the reciprocal hexagonal lattice is $1.12\,nm^{-1}$, corresponding to 1.03 nm in the real space. (c) Zoom of panel (a) showing the boundary between two hexagonal domains. The white parallelograms indicate the unit cells. Image size is $14 \times 14\,nm^2$. (d) STS curve obtained by averaging 30 spectra acquired on 1 ML $C_{60}/Cr_4O_5/Fe$.

The electronic structure of the spinterface was also investigated by means of PES. Selected PES spectra related to 1 molecular layer of C_{60} on Fe(001), Fe(001)-$p(1 \times 1)$O, and Cr_4O_5/Fe have already been discussed in previous publications.[8,12] In Fig. 2, we present a set of normal emission PES spectra related to the $C_{60}/Cr_4O_5/Fe$ system, by reporting them as a function of molecular coverage. The Cr_4O_5/Fe substrate spectrum, displayed in the bottom row, is characterized by a metallic Fermi edge and by a large peak located at a binding energy of −4.9 eV. The latter, which is related to oxygen states, is reminiscent of a similar peak that characterizes the PES spectrum of the Fe(001)-$p(1 \times 1)$O substrate (not shown here) as discussed in Ref. 16.

Molecular peaks start to appear already in the submonolayer coverage regime and become well-defined at the completion of the first molecular layer. At this stage, the HOMO peak is centered at −1.7 eV from E_F. This HOMO position reveals the occurrence of a significant charge transfer, which is estimated to be about 1.5 electrons per molecule, as discussed below, on account of a relatively strong interaction with the metallic substrate. The strength of the interface coupling also reflects in a small shift of about 0.15 eV of the oxygen related peak (formerly at −4.9 eV) toward lower binding energy, in good agreement with the donor role played by the substrate.

The green spectrum is related to 1 ML of C_{60} deposited on Fe(001)-$p(1 \times 1)$O, which is shown here as a reference. In the latter

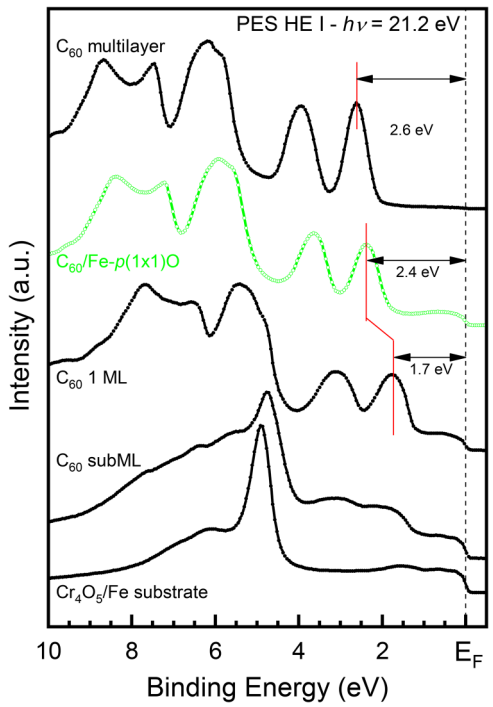

FIG. 2. Photoemission spectra ($h\nu = 21.2\,eV$) acquired at normal emission on the $Cr_4O_5/Fe(001)$ substrate (bottom spectrum) and after C_{60} deposition with increasing coverages (from bottom to top), as indicated. The spectrum related to 1 ML $C_{60}/Fe(001)-p(1 \times 1)O$ (green dots) is also reported, for reference.

case, the interface coupling was observed to be weaker so that the peak positions are close to those observed in multilayer films that, being characterized by the weak van der Waals interaction between adjacent layers, are representative of a fullerene layer poorly interacting with the substrate. It is worth noticing that in the spectra related to 1 ML of C_{60}, the substrate DOS close to E_F is still visible, thus ensuring a correct setting of the binding energy scale.

Finally, a spectrum related to a multilayer C_{60} film on Cr_4O_5/Fe is shown in the upper row of Fig. 2. As discussed above, the lineshape and the peak positions here are consistent with those typical of fullerene layers on poorly interacting substrates. Also, features related to the substrate are no longer visible.

According to our *ab initio* calculations, the most stable configuration among those analyzed is for C_{60} adsorbing through a C–C bond on top of a Cr atom ("bond/Cr" in the following). The corresponding geometry is reported in Fig. 3(a), in which the squared unit cell is reported (dashed line) in comparison with that of the clean surface (solid line) and the adsorption position is marked by an arrow. The height of the C–C bond over the Cr atoms plane is 2.74 Å, corresponding to a C–Cr equilibrium distance of 2.80 Å [see Fig. 3(b)].

This configuration is stabilized by the interaction between the π orbitals of C_{60} and the d states of Cr, as can be evidenced by looking at Fig. 3(c). There, the adsorption charge displacement is reported, $\Delta\rho = \rho_{mol/surf} - \rho_{mol} - \rho_{surf}$, where $\rho_{mol/surf}$, ρ_{mol} and ρ_{surf} are the electron densities of the full system, the C_{60} molecules, and the clean surface, respectively, all computed with the same atomic configurations. Electron density accumulates in the region between the C–C bond and the Cr atom.

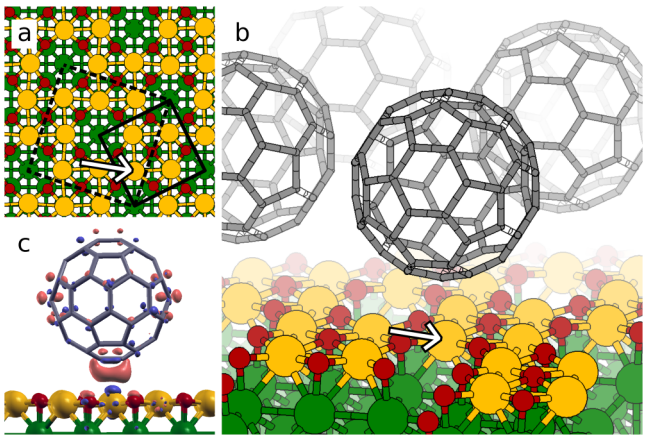

FIG. 3. (a) Ball-stick model of the pristine surface showing the $(\sqrt{5}\times\sqrt{5})$–R26.6° reconstruction (solid line) and the $(\sqrt{10}\times\sqrt{10})$–R(−18.4°) supercell used in the simulations (dashed line). Small dark (red) spheres are used for showing O atoms, large bright (yellow) spheres for Cr ones, and large dark (green) spheres for Fe atoms. (b) C_{60} (gray wireframe) adsorbed by a C–C bond on top of a Cr atom [see the arrows in panels (a) and (b)], the most stable adsorption configuration identified as optimized by DFT. (c) Electron density displacement upon adsorption, $\Delta\rho = \rho_{mol/surf} - \rho_{mol} - \rho_{surf}$ showing increase (red) and depletion (blue) of electron density at isovalue $\Delta\rho = \pm 0.01$ Å^{-3}.

Some predominant increase of electron density can also be appreciated (red lobes). This can be estimated by the Löwdin charges: we find that upon adsorption, the molecule gets negatively charged (by adding 1.55 e^-), mostly at the expense of O atoms (with a variation of −0.75 e^- per unit cell), then Cr atoms (−0.44 e^-/unit cell), and Fe ones (−0.34 e^-/unit cell). It should be noted that the Cr atom below the C–C bond [arrow in Figs. 3(a) and 3(b)] is computed to have a very similar charge state (−0.066 e^-/atom) to the average of the Cr atoms (−0.055/atom). This indicates that the interaction of C_{60} with the surface, in addition to the localized covalent bond, involves many atoms surrounding the molecule, each one participating to the charge displacement.

The second most stable adsorption configuration is again by the C–C bond, but at a Cr vacancy, and it is 0.7 eV higher in energy than the bond/Cr configuration discussed so far. The same molecular orientation at an O site has even higher energy (≈4 eV). Looking instead at different molecular orientations at the Cr site, a molecule facing the substrate with a hexagonal face is 2.1 eV more energetically expensive than that facing the substrate by exposing the C–C bond; the energetic cost further increases to 3.2 eV for a C_{60} molecule facing the Cr atom with a pentagonal face. Clearly, these adsorption configurations cannot be stabilized by the same mechanism (interaction of one π bond with the Cr states) available for the bond/Cr configuration. Indeed, for a molecule facing the substrate by a hexagon it would be more convenient to adsorb at a vacancy site (that we found to be the third most stable configuration, at +1.1 eV).

Coming back to the electronic properties of the system in its optimized geometry (bond/Cr), in Fig. 4(a), we report the spin polarization (the difference $\rho_{up} - \rho_{dw}$, where Fe is magnetized "up"). This shows that the magnetization of the Cr layer (negative valued blue isosurfaces) is opposite to the one of iron (positive valued red isosurfaces), as expected for the clean surface. Also,

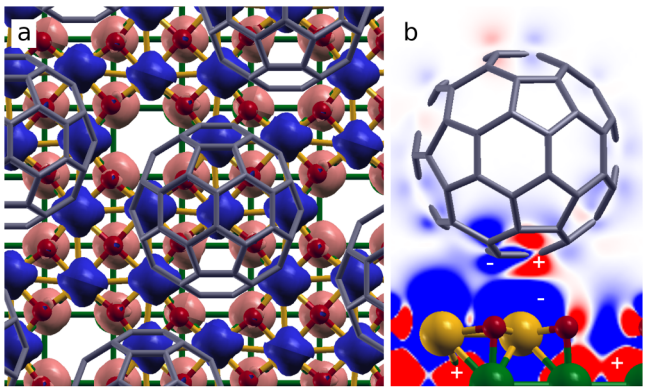

FIG. 4. Spin polarization in the bond/Cr geometry. (a) Top view of the system with isosurfaces set to ±0.1 Å^{-3}. (b) Side view with color scale, maximum values set to ±0.002 Å^{-3} to better highlight the contribution on the molecule. Brighter (red) and darker (blue) regions correspond to positive (spin-majority) and negative (spin-minority) polarization, respectively, as further indicated by +/− signs in panel (b).

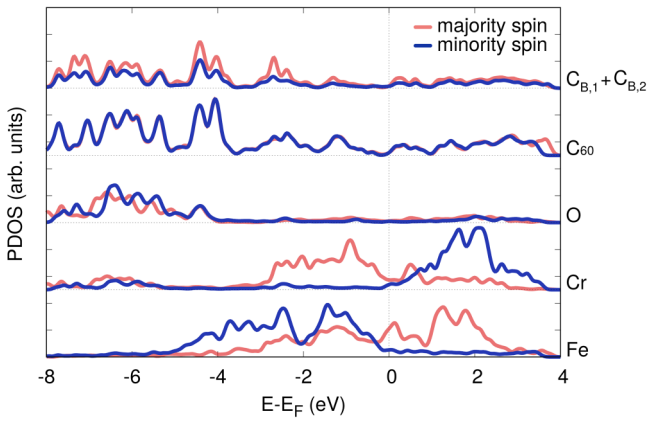

FIG. 5. Density of states projected on different atoms and summed over the Fe substrate, the Cr layer, the O atoms, the C_{60} molecule, and the two carbon atoms facing to the surface, from bottom to top. Curves are stacked for clarity.

most magnetization in the ground state lies in the substrate, while the molecule is much less affected. Nevertheless, a mild spin polarization is induced in C_{60} by interaction with the substrate, as can be appreciated when a smaller isovalue of the spin polarization is considered, especially for those atoms of the molecule that are closer to the surface, as reported in Fig. 4(b).

Similar but more quantitative information can be deduced by the density of states projected on different atoms (PDOS), which is reported in Fig. 5. The two lowest panels show the antiferromagnetic alignment of Cr and Fe, while in the third one, the small spin polarization of oxygen atoms can be appreciated, as discussed in our earlier work.[16] Notably, the binding energy of the oxygen-related features is in good agreement with the peak observed in the PES. The two upper panels of Fig. 5 display the PDOS on the C_{60} molecule and the contribution to the PDOS summed over the two carbon atoms facing to the surface. The molecular features are compatible with the peaks observed in the PES at −1.7 eV, −3.0 eV, and −5.0 eV. The magnetization on the whole molecule is negligible on this scale. Differently, the two carbon atoms directly involved in the interaction with the substrate show a mild spin dependence of the DOS. Still, they are characterized by a small spin polarization parallel to one of the Cr atoms and amounting to 0.004 for the C atoms pointing towards a Cr, while the C atom closer to the vacancy displays a smaller spin polarization (−0.0019) parallel to that of the iron substrate. These results demonstrate that there is a proximity effect of the substrate on the molecule, inducing a magnetic moment on carbon atoms which depends on the local environment.

IV. CONCLUSIONS

In conclusion, we have focused our attention on a specific spinterface, formed by the coupling between C_{60} fullerene and the two-dimensional magnetic oxide Cr_4O_5, stabilized onto the Fe(001) substrate.

Such a system appears to be very interesting as it combines a significant electronic interaction, which is necessary in order to generate spin-polarized hybrid interface states, with a growth mode characterized by a high degree of order of the overlayer, which can form a compact fullerene monolayer. Both characteristics are promising in view of applications, where the interface states might play an active role in mechanisms such as spin filtering, while the possibility of growing compact molecular layers would be favorable for the realization of layered structures.

The *ab initio* calculations have offered further insights into the nature of this spinterface by determining the interaction and charge transfer between fullerene and substrate, and the spin-polarized electronic states. Simulations appeared to substantially agree with the experimental observations, thus crucially supporting them.

ACKNOWLEDGMENTS

We acknowledge the CINECA award under the ISCRA initiative, for the availability of high performance computing resources and support (Application No. HP10C2SVDP).

REFERENCES

[1]S. Sanvito, Chem. Soc. Rev. **40**, 3336 (2011).
[2]V. A. Dediu, L. E. Hueso, I. Bergenti, and C. Taliani, Nat. Mater. **8**, 707 (2009).
[3]G. Szulczewski, S. Sanvito, and G. Coey, Nat. Mater. **8**, 693 (2009).
[4]M. Cinchetti, V. A. Dediu, and L. E. Hueso, Nat. Mater. **16**, 507 (2017).
[5]C. Barraud, P. Seneor, R. Mattana, S. Fusil, K. Bouzehouane, C. Deranlot, P. Graziosi, L. Hueso, I. Bergenti, V. Dediu, F. Petroff, and A. Fert, Nat. Phys. **6**, 615 (2010).
[6]M. Bibes, J. E. Villegas, and A. Barthélémy, Adv. Phys. **60**, 5 (2011).
[7]G. Szulczewski, H. Tokuc, K. Oguz, and J. M. D. Coey, Appl. Phys. Lett. **95**, 202506 (2009).
[8]A. Picone, D. Giannotti, M. Riva, A. Calloni, G. Bussetti, G. Berti, L. Duò, F. Ciccacci, M. Finazzi, and A. Brambilla, ACS Appl. Mater. Interfaces **8**, 26418 (2016).
[9]R. Bertacco and F. Ciccacci, Phys. Rev. B **59**, 4207 (1999).
[10]F. Donati, P. Sessi, S. Achilli, A. Li Bassi, M. Passoni, C. S. Casari, C. E. Bottani, A. Brambilla, A. Picone, M. Finazzi, L. Duò, M. I. Trioni, and F. Ciccacci, Phys. Rev. B **79**, 195430 (2009).
[11]A. Picone, G. Fratesi, A. Brambilla, P. Sessi, F. Donati, S. Achilli, L. Maini, M. I. Trioni, C. S. Casari, M. Passoni, A. Li Bassi, M. Finazzi, L. Duò, and F. Ciccacci, Phys. Rev. B **81**, 115450 (2010).
[12]A. Brambilla, A. Picone, D. Giannotti, A. Calloni, G. Berti, G. Bussetti, S. Achilli, G. Fratesi, M. I. Trioni, G. Vinai, P. Torelli, G. Panaccione, L. Duò, M. Finazzi, and F. Ciccacci, Nano Lett. **17**, 7440 (2017).
[13]A. Picone, A. Brambilla, A. Calloni, L. Duò, M. Finazzi, and F. Ciccacci, Phys. Rev. B **83**, 235402 (2011).
[14]A. Picone, G. Fratesi, M. Riva, G. Bussetti, A. Calloni, A. Brambilla, M. Trioni, L. Duò, F. Ciccacci, and M. Finazzi, Phys. Rev. B **87**, 085403 (2013).
[15]A. Brambilla, G. Berti, A. Calloni, A. Picone, M. Riva, G. Bussetti, S. Nappini, E. Magnano, M. Finazzi, L. Duò, and F. Ciccacci, J. Appl. Phys. **114**, 123905 (2013).
[16]A. Calloni, G. Fratesi, S. Achilli, G. Berti, G. Bussetti, A. Picone, A. Brambilla, P. Folegati, F. Ciccacci, and L. Duò, Phys. Rev. B **96**, 085427 (2017).
[17]G. Berti, A. Calloni, A. Brambilla, G. Bussetti, L. Duò, and F. Ciccacci, Rev. Sci. Instrum. **85**, 073901 (2014).
[18]T. Thonhauser, S. Zuluaga, C. A. Arter, K. Berland, E. Schröder, and P. Hyldgaard, Phys. Rev. Lett. **115**, 136402 (2015).

[19]V. R. Cooper, Phys. Rev. B **81**, 161104(R) (2010).
[20]D. Vanderbilt, Phys. Rev. B **41**, 7892 (1990).
[21]P. Giannozzi, S. Baroni, N. Bonini, M. Calandra, R. Car, C. Cavazzoni, D. Ceresoli, G. L. Chiarotti, M. Cococcioni, I. Dabo, A. D. Corso, S. de Gironcoli, S. Fabris, G. Fratesi, R. Gebauer, U. Gerstmann, C. Gougoussis, A. Kokalj, M. Lazzeri, L. Martin-Samos, N. Marzari, F. Mauri, R. Mazzarello, S. Paolini, A. Pasquarello, L. Paulatto, C. Sbraccia, S. Scandolo, G. Sclauzero, A. P. Seitsonen, A. Smogunov, P. Umari, and R. M. Wentzcovitch, J. Phys. Condens. Matter **21**, 395502 (2009).
[22]H. J. Monkhorst and J. D. Pack, Phys. Rev. B **13**, 5188 (1976).
[23]T. Sakurai, X.-D. Wang, Q. Xue, Y. Hasegawa, T. Hashizume, and H. Shinohara, Prog. Surf. Sci. **51**, 263 (1996).